Chen Duanduan (Orcid ID: 0000-0002-5706-4369)

Optimization Schemes for Endovascular Repair with Parallel Technique based on Hemodynamic Analyses

Huanming Xu[1], Yuqian Mei[2], Xiaofeng Han[3], Jianyong Wei[1], Paul N. Watton[2], Wan Jia[4], Anqiang Li[5], Duanduan Chen[1]* and Jiang Xiong[6]*

[1]School of Life Science, Beijing Institute of Technology, Beijing, China.

[2]Department of Computer Science & INSIGNEO Institute, University of Sheffield, UK.

[3]Department of Diagnostic and Interventional Radiology, Beijing Anzhen Hospital, Capital Medical University, China.

[4]Department of Vascular Surgery, The Second People's Hospital of Yunnan Province, Kunming, China.

[5]Department of Vascular Surgery, Gansu Provincial People ' s Hospital, Lanzhou, China.

[6]Department of Vascular and Endovascular Surgery, Chinese PLA General Hospital, Beijing, China.

Corresponding author: Prof Duanduan Chen

School of Life Science, Beijing Institute of Technology

Beijing, 100081, China.

Tel. +86-10-68912154

Fax. 86-10-68912154

Email. duanduan@bit.edu.cn

Dr Jiang Xiong

Department of Vascular and Endovascular Surgery,

Chinese PLA General Hospital, Beijing, 100853, China.

Tel. +86-10-66938349

Email. xiongjiangdoc@126.com

Abstract

Endovascular repair with parallel stent-grafts (SG) is a challenging technique that reconstructs the luminal flow pathways by implanting parallel-placed SGs into the vessel. After treatment, occlusion and shifting of the parallel SGs are sometimes reported, which could be fatal and difficult to be re-operated. These issues are highly related to the local hemodynamic conditions in the stented region. In this study, a patient case treated by octopus endograft technique (a head-SG with three limb-SGs) and experienced limb-SG occlusion is studied. 3-D models are established based on CT-angiography datasets pre- and post-treatment as well as during follow-ups. Hemodynamic quantities such as pressure drop, wall shear stress-related parameters and flow division in limb-SGs and visceral arteries are quantitatively investigated. Optimizations on the length of the head-SG and diameter of the limb-SGs are analyzed based on various scenarios. The results indicate that when reconstructing the flow pathways via octopus stenting, it is important to ensure the flow distribution as physiological required with this new morphology. Position (or length) of the head-SG and diameter of the limb-SGs play an important role in controlling flow division, and high TAWSS around the head-SG acts as a main factor for graft immigration. This study, by proposing optimization suggestions with hemodynamic analyses for a specific case, implicates that pre-treatment SG scenarios may assist in wise selection and placement of the device and thus may improve long-term effectiveness of this kind of challenging endovascular repair techniques.

Key words: octopus endograft technique, hemodynamic, optimization scenarios

1 | INTRODUCTION

Endovascular repair is widely used in treating vascular diseases. It implants stent or stent-graft into the vessel to divert flow or expand the collapsed lumen [1, 2]. For treatment in main vasculatures, the operation sometimes involves modified or multiple stent-grafts (SGs). SG strategies such as chimney, snorkel, periscope, sandwich and other parallel techniques are often used in vasculatures with branches in order to maintain the hemodynamic function of each flow pathway [3-6]. Among them, octopus technique, which implants parallel-placed SGs into one vessel to convert the single lumen into multiple flow paths, is a challenging procedure and plays an important role in treating patients who are not available for open surgery and require reconstructing of vessel branches[7].

The efficacy of parallel SG technique, especially for the octopus strategy, has been investigated from the clinical aspect [8-12]. A few suggestions on wise treatment plan have been proposed. Rafael and colleagues proposed a preferable combination of Viabahn stent sizes to be used in octopus technique based on CT measurement [13]. Mestres *et al.* established *in vitro* analysis to reveal the hemodynamic conditions for parallel stenting [14]. Moreover, in the study by Lepidi and colleagues, eighteen patients were successfully treated via parallel endografts, confirming the effectiveness and feasibility of parallel SG placement as a straightforward technique in the treatment with complicated patients [15].

In addition to clinical practice, computational hemodynamics has been increasingly used in analyzing vascular diseases. Regular planning of the stenting technique in main vasculatures has been widely studied, especially for aneurysms [16-20] and aortic dissections [21-24]. However, to the best knowledge of the authors, computational analyses regarding parallel SG technique are still lacking. Investigating this challenging stenting technique from hemodynamic aspect would contribute to better understandings about the pros-and-cons of this technique and thus assist in directing pre-treatment personal plans to improve the safety and effectiveness of the treatment.

In this study, we established computational models based on CT-angiography (CTA) datasets (pre- and post-treatment with follow-ups) from a patient who was treated by octopus SG technique [25]. By solving the three-dimensional unsteady conservation equations for mass

and momentum, we provide detailed information on hemodynamics of the modified arterial system. Moreover, stenting scenarios by modifying the length and diameter of SG selection are analyzed, in order to provide suggestions on better SG arrangement for this kind of complicated stenting technique.

2 | Materials and methods

2.1 | Patient and image acquisition

A 46-year-old man with type-B aortic dissection was admitted with a 10-month history of rapidly expanding false lumen (FL) and was afflicted by 6-month intermittent dull pain in the upper back and left lower extremity claudication. The patient refused open surgery or hybrid repair. With the approval of institutional review board and the signed informed consent, octopus endograft technique was used to reconstruct the affected aorta with renovisceral arteries and to prevent further enlargement of FL. Details regarding the octopus SG technique and the specific SGs that were used can be found in [25].

The patient was experienced two CTA scans before the octopus SG implantation (after thoracic endovascular aortic repair) and three CTA examinations during one-year follow-ups via a dual-source CT scanner (Brilliance iCT256, Royal Philips, Dutch). The reconstruction parameters of the CT scan include: helix acquisition, Matrix 512x512mm, slice thickness 1mm, kVp 100kV, and FoV 350.00mm. Representative CTA images in thoracic aorta region with octopus technique are shown in Fig.1a.

2.2 | 3-D reconstructed models

Segmentation on CTA image datasets and 3-D reconstructions of aortic models were accomplished via Mimics (Materialise, Belgium). In order to ensure the 3-D models presenting the actual contour of the vessel lumen, the cross-sectional contours of the reconstructed geometries were mapped back to CTA images and were reviewed by experienced vascular surgeons (Fig 1b). Based on CTA datasets, a total of five models were reconstructed, including two pre-octopus models and three post-octopus ones. As shown in Fig.2a (pre-octopus 11months), the patient was firstly treated by thoracic endovascular aortic repair with

implantation of a thoracic SG to seal the primary entry. Both of the true and false-lumen (TL and FL) of this patient acts as flow pathways to perfuse downstream artery. The TL connects to the right renal artery and the iliac artery, while the FL connects to the celiac artery (CA), superior mesenteric artery (SMA), left renal artery (LRA) and iliac artery. After 10-month time, the distal perfusion pathway of FL to the iliac artery was blocked (Fig.2b), changing its tubular shape into the saccular one and inducing potential risk of rupture. To prevent further expansion of FL, octopus technique was applied. As shown in Fig.2c (post-octopus 1week), a SG with 16x16x120mm was implanted into the FL to serve as the octopus head (head-SG) and three endografts are then parallel placed into this head as the limb-SGs. Each of them has been extended by two other endografts until the pathway reaches the visceral arteries. In this case, the three limb-SGs perfuse CA, SMA and LRA, respectively, and are named accordingly as PSG-1, -2 and -3 (Fig.2c). A few months later, occlusion of PSG-1 and -3 occurred. Although imaging and physiological indicators did not present distal vascular diseases or problems in liver or kidney functions, at this moment, the flow condition of the patient was dramatically disturbed (Fig.2d-e).

2.3 | Numerical models

Each 3-D model was discretized in ICEM (ANSYS Inc, Canonsburg, USA) with tetrahedral elements in the core region and prismatic cells in the boundary layers near the aortic wall. The grid resolution varies from 1.4-2.0 million cells. The heart-beat cycle was measured and the averaged value was 67 beats /min for this patient. Temporal discretization of numerical models was assigned as 50 steps per cycle. Grid and independency analyses on finer grids and temporal discretization were conducted which proves that the base mesh resolution and time step settings were adequate in this study. Details are presented in S1, supplementary material.

The blood was assumed as incompressible with density of 1044 kg/m^3 and dynamic viscosity of 0.00365 kg m^{-1} s^{-1}. Newtonian model was applied, due to the relative high shear rate in the aortic system[26-28]. Based on the equivalent diameter ($D_e = 2\sqrt{Area/\pi}$) and velocity at the inlet of the ascending aorta pre- and post-treatment, the average Reynolds number over a cardiac cycle can be calculated as 4540-5791. It was confirmed in our previous study that

laminar simulations with adequately fine mesh resolutions, especially refined near the walls, can capture flow patterns [24]. A finite volume solver, CFD-ACE + (ESI Group, France) was employed in this study to solve the transport equations - Navier-Stokes equations, together with the continuity equation of incompressible and Newtonian fluid (Eq.1-2), where u stands for velocity, ρ stands for density, μ represents dynamic viscosity, and P denotes pressure. ~~A second order accurate discretization (central differences) was used to solve the flow velocity.~~ For each time step, 500 iterations were conducted. The residual criteria was assigned as 10^{-18}, and the actual convergence was confirmed by the flatten pattern of the residual plot. For each model, four cardiac cycles simulations were carried out to obtain a periodic solution, and the results of final cycle were presented for post-processing and analysis.

$$\nabla \cdot (u) = 0 \tag{1}$$

$$\rho \left(\frac{\partial u}{\partial t}\right) + \rho(u \cdot \nabla)u = -\nabla P + \mu \nabla^2 u \tag{2}$$

2.4 | Boundary conditions

For this study, boundary conditions of the computational models include aortic wall, velocity and pressure boundaries. Owing to low distensibility of aorta/arteries in patients with aortic dissection and SGs, the vessel wall was considered no-slip and rigid. Velocity boundaries were assigned for inlet of ascending aorta (AA) and outlets of brachiocephalic trunk (BT), left common carotid artery (LCCA) and left subclavian artery (LSA, which is only available in the comparison case on a healthy aorta). Since the blood pressure of the patient during follow-up was strictly controlled, the cardiac output of the patient was reported as normal condition, and we focused on the flow patterns in the descending aorta and the downstream section, velocity boundaries were assign as the data extracted from healthy volunteers. In detail, twenty volunteers were measured using Doppler ultrasound velocimetry; the data of the inflow at AA and outflow at BT and LCCA were applied to the computational models. Centerline velocity of AA inlet was achieved by measurements through the apical 5-chamber view and the suprasternal long axis view of the aortic arch. For other arteries (BT, LCCA and LSA), Doppler velocimetry has been conducted at the proximal and distal sites of the targeted vessels. The measured velocities are considered effective if the difference between the two measurements

for each vessel is less than 5%. Time-variant maximum velocity at the measured site was then extracted from the upper edge of the velocity sonogram (Fig.1c). As the velocity boundary conditions, the flow rates at AA, BT, LCCA and LSA can be calculated based on the measured time-variant maximum velocity and the assumed flat flow profile for AA and parabolic flow profile for the others. In fact, there is strong secondary flow occurred in the root of AA, however, this flow pattern may have less effects on the descending aorta and the distal region than the region close to AA [29]. Most studies focused on type-B aortic dissection neglected it and assigned flat velocity profile at the aortic inlet [30-32]. The flow rates over a cardiac cycle were calculated from the measured data of twenty volunteers for each velocity boundary. Fig.1d shows the velocity curves during one cardiac cycle assigned to AA, BT, LCCA and LSA for these models. Pressure boundaries were applied on the outlets of the celiac artery, superior mesenteric artery, renal arteries and common iliac arteries. These outlets in the models have been assigned as extension with zero pressure at the distal extension ends [33]. Each pressure outlets were extended by 25-times of the diameter of the corresponding outlets and zero pressure was assigned to the extended ends. By this means, the distal resistance could be partially simulated. impedance of the distal vessels to the organs might be taken into account and different impedances could be considered by the various extension lengths based on the specific diameters of the outlets in the original models.

2.5 | Optimization scenarios

The follow-up examinations show occlusion of the limb-SGs, the occurrence of which can be analyzed by hemodynamic analysis and suggestions that may improve the hemodynamic environment by modifying the SGs can be discussed. Basic flow analysis on the original plan of SGs implies inappropriate flow division in each arterial branch, thus, optimization schemes are studied in this study by modifying the octopus SG set via Geomagic Studio (3D System, USA) to investigate various flow conditions. As shown in Fig.2f, the reconstructed model based on the first CTA scan after octopus treatment is used as the base model for modification. In the first scenario (Length-scenario), the length of the head-SG is extended to analyze the influence of the beginning position of parallel limb-SGs on flow perfusion for the vascular system. Eight

models with various extending length of head-SG are studied (2-10cm) and shown in Fig.2g. Taking the flow proportion in each pathway as the optimization goal, the best extending length is selected, and based on that selected model, the second SG modification scenario on diameter (Diameter-scenario) can be investigated. The diameters of limb SGs are then varied by 1-2mm (further reduction is not suitable for this specific case) to adjust visceral perfusion (Fig.2h). Suggestions of wise SG placement for similar patient case can be then proposed, as far as the flow division is concerned.

3 | Results

3.1 | Hemodynamic analysis of the patient

The flow perfusion in patients with type-B aortic dissection can be dramatically disrupted by the establishment of FL. In some patients, direct perfusion to the viscera or even lower limbs can be substituted by FL. In the particular patient we studied, after the first interventional treatment with an aortic SG sealing the primary entry, the TL and FL are still existed and respectively supply flow to the right renal artery and the lower limbs (TL) and to the CA, SMA and LRA (FL). Fig.3a shows the velocity streamlines for each pre- and post-octopus treatment cases at systolic peak. The flow is generally organized when examined just post-TEVAR. The FL plays an important role in perfusion to visceral arteries and the left lower limb. In the second examination post-TEVAR (pre-octopus 1month), closure of the FL disturbs flow towards the limb and vortical flow is presented in the sac near the visceral arteries (arrow indicated). Besides, higher velocity is found in TL and visceral arteries. After octopus treatment, flow velocities in TL and in PSG-2 increase; while vortical flow is found in PSG-1 and reduced flow is found in PSG-1 and -3. In one-year post-octopus, PSG-1 and PSG-3 were closed and high velocity can be still observed in PSG-2. Flow velocities, at systolic peak, in the region below the TL-FL bifurcation and above the visceral arteries (as shown by the blue square in Fig.3a) are recorded for each case. The averaged velocity in this region for the post-octopus models is calculated by the integral of the velocity based on the volume and then dividing it with the volume of the vessel segment. The variation of them is shown in Fig.3b. It is obvious that the average velocity in PSG-1 and PSG-3 of this volume was relative low compared with PSG-2.

The average velocity in PSG-1 of this area declined dramatically before it was occluded, which contributes to the thrombosis in this branch.

Apart from velocity streamlines, loading pattern is also crucial for hemodynamic analysis of vessel remodeling. Fig.4 shows the relative residence time (RRT) and time average wall shear stress (TAWSS) distributions in the three limb-SGs. It can be found that, after octopus treatment, high RRT is found in the proximal region of PSG-1 and middle region of PSG-3, indicating possible surface thrombosis in these lumen. High TAWSS is found at the proximal region of the PSGs, and a sharp loading drop can also be found at the root of PSG-3, indicating flow impact in this region and danger of SG transposition. The average pressure drop from ascending aorta to the abdominal region during a cardiac cycle for the pre- and post-octopus models are 3.41mmHg, 12.1mmHg, 19.4mmHg, 17.1mmHg and 25.7mmHg respectively according to the examination history; while the average pressure drop over a cardiac cycle for the normal case is 1.60mmHg, implicating the implanted PSGs may greatly influence the loading condition in their upstream.

Table1 shows the averaged flow division to aortic branches during a cardiac cycle. The perfusion in the first-examined model (pre-octopus 11months) is similar as the computation of normal aorta. However, since the left common iliac artery (CIA) is occluded at the second examination (pre-octopus 1month), the perfusion in visceral arteries and right CIA varies greatly; CA and SMA take more than 30% of the inflow of ascending aorta, and the perfusion to the lower limbs is largely reduced. After octopus treatment, the perfusion to the branches does not improve. The occlusion of PSG-1 and -3 in the following examinations may be related to the abnormal flow perfusion to the visceral and limb arteries.

3.2 | Optimization scenarios and hemodynamic features

In order to improve the flow condition induced by the parallel stents, optimization scenarios were investigated. The Length-scenario is firstly applied by extending the head-SG; then, based on the optimized length, Diameter-scenario is studied by varying the diameter of the limb-SGs (Fig.2f-h). By extending the head-SG with 2-10cm, Fig.5a shows pressure distribution of the cases in Length-scenario at systolic peak. The results indicate that the pressure drops from the

ascending aorta to the downstream more smoothly in the cases with extended SG-head. Further, the pressure drop from the inlet of ascending aorta to the outlets of CIAs over a cardiac cycle of each case is quantified (Fig.5b). It indicates that the pressure drop decreases significantly when the SG-head is extended from 2cm to 4cm. Although the pressure drop continues to decrease as the SG-head further extended, the variation is trivial (less than 8.2% with extension of 5-10cm). Fig.5c shows the variation of flow proportion to the FL in these cases. It increases from 41.7% to 48.9%, when the SG head is extended from 2 to 4cm, and increases slightly with further extension (5-10cm). Indeed, the FL supplies flow to the CA, SMA and LRA. The flow proportion for them in the normal aorta is 20.76%; thus, increasing of the FL flow proportion is not supportive for maintaining the nature visceral blood supply. Detailed flow proportions to aortic branches are listed in Table 2.

Combining the results of pressure drop and flow division, Length-scenario with extension of SG head by 4cm is selected as the optimization, and it is applied for Diameter-scenario. Due to the exceeded flow portion to the FL, the diameters of PSG-1 and -2 are modified to simulate treatment with smaller diameters of body grafts. As shown in Fig.5d, by reducing the diameter of both body grafts by 1 and 2mm respectively, the flow entering the limb SGs is improved. As quantified in Table 2, by comparing to the perfusion of the control model, the flow proportion is improved in the model with 2mm-diameter reduction.

4 | Discussion

Parallel endografts has been increasingly used in endovascular repair for main vasculatures, especially for patients cannot be treated by conventional vessel interventions or open surgery [14]. However, there are still some concerns regarding using parallel stenting technique, including the incidence of endoleak and occlusion of the stents, and failure to reconstruct natural flow division in branches [14, 33]. In addition, there is no obvious evidence to show that which combination of endograft and parallel graft is the best [34]. In the present study, a longitudinal study of a patient experienced treatment with octopus technique [25] is conducted. By analyzing the flow and loading conditions of this patient, we reveal flow and loading distributions are unsatisfactory during the follow-ups and suggest this might be one of the main

factors for the failure of this treatment. Thus, Length and Diameter-scenarios are investigated in order to propose optimized plans of this complicated stenting treatment and provide suggestions for future similar operations.

Based on this longitudinal study, the value of TAWSS around the root of PSG-1 is relatively high, indicating a higher drag force occurred on this PSG. Besides, stenosis is found in the PSG-1 and -3, inducing relatively low pressure distributions around these regions, disturbing the flow entering the target visceral arteries. This might be one of the main factors that result in thrombosis near this area, and thus leads to the occlusion in PSG-1 and -3 before the last follow-up. Furthermore, the percentage of flow entering into SMA was 33.4%, while only 8.75% of total inflow from the ascending aorta entering into SMA in the control model (Table 1), which means such morphology of the post-octopus (1 week) model might not be able to maintain a natural visceral perfusion.

The pressure drop from the ascending aorta to the outlets of common iliac arteries over a cardiac cycle is quantified in each model. The pressure drop in the original model of post-octopus (1 week) is 19.4mmHg; while it is 1.60mmHg in the control model. By extending the length of the head-SG, the pressure drop can be gradually decreased. It is decreased by approximately 32.0% with extension of the SG head by 4cm; while with further extension, the pressure drop keeps a decreasing tread but with trivial magnitude variation (13.2-11.9mmHg). At the same time, with the extension of SG-head, blood flow entering into the original FL increased (Fig 4c), which results in more blood flowing into the three PSGs and induces abnormal visceral perfusion. Therefore, another optimization scenario is needed.

Compared with the case L-4cm, the proportions of flow entering into each branch (CA, SMA, LRA) were closer to their counterparts in control model, and the perfusion in case D-2mm is better than that in case D-1mm (Table 2). The results indicate that the diameters of PSG-1 and PSG-3 selected in this patient might not the best. Although the pressure drop in case D-1mm (19.1mmHg) and in D-2mm (25.2mmHg) are larger than that in L-4cm (13.1mmHg), the optimization scenario D-2mm was treated as the best one among all of the scenarios considering both pressure drop and perfusion in this study. In fact, further reduction of the diameter of PSG-1 and PSG-3 may mismatch the studied vessel.

One of the most important advantages of parallel endograft octopus technique is that individual customization is not necessary [35]. Thus, in clinical operations, octopus grafts are often constructed based on available device, and more importantly, selection of length and diameter of the SGs is possible. Although the octopus technique can be successful applied in a number of patients [7, 25, 36], its mid- and long-term outcomes need to be further determined and stenting plan needs to be quantitatively studied [37]. In the current patient case, the prognosis is not satisfactory in long-term follow-up. Based on hemodynamic analysis, the occlusion of the two limb-SGs is proposed to be related to the local loading conditions and visceral flow divisions. Both of the conditions can be simply improved by extending the length of the head-SG and reducing the diameter of the limb-SGs. Based on this study, it can be confirmed that maintaining the nature flow division and pressure distribution is important for the octopus vascular reconstruction. Hemodynamic analysis can contribute to predicting and evaluating the post-treatment results, and thus, providing suggestions on wise selection of the combination of SGs for vascular reconstruction.

5 | Limitations

This study was conducted based on multiple follow-up data of a patient case operated by octopus stenting. Indeed, solid medical conclusions should be better determined by involving a greater number of patient cases. However, patients with complex parallel stenting are not common and the conditions of them are highly individualized. Based on the current patient case, this study preliminarily shows the importance of maintaining hemodynamic conditions in the vasculature and proposes suggestions on selection and placement of endografts, which might be helpful in treatment plan for future complicated stenting operations with multiple and parallel stenting. This study also suffers from limitations of patient-specific boundary conditions and the lacking of fluid-wall interaction analysis. Indeed, computational studies with individualized parameters would be good to reflect the actual flow situations; however, in most conditions, velocimetry and intraluminal pressure measurements are not available. A summary of the boundary conditions in recent computational studies is presented in S2, supplementary material. In this study, extended outlets have been applied in the model to partially take account

of the distal resistance, however, the compliance of the distal vessels have not been considered. Besides, most regions of the aortic system of the patient have been reconstructed by stents, thus, the distensibility of the aortic wall is weak and the interaction between the wall and the blood flow was neglected. More accurate quantitative results would be achieved when detailed patient-specific boundary data is available, but we believe, the current study may still reflect a few flow features generated by the morphology of the aorta. Furthermore, the secondary flow at the root of the aorta was ignored in this study as it might take less influence on the flow in the descending aorta than that in the ascending aorta. At last, this is a retrospective study, reviewing the flaws of the stent design in a post-operated patient. It emphasizes the importance of diameter and position selections of the device, but more valuable studies should be conducted on prospective cases to direct stenting plan.

6 | Conclusions

In this study, morphological and hemodynamic factors that induce the unsatisfactory prognosis of the studied patient have been investigated. A serial of optimization scenarios were presented to improve the perfusion and pressure distributions. The results indicate that, for this particular case, by extending the head-SG with 4cm and reducing the limb-SGs by 2mm, the flow and loading conditions of the reconstructed aortic system can be greatly improved. This indicates that pre-treatment planning on wise selection of the length and diameter of SGs is important for the parallel stenting treatment; it should be considered for future treatments to improve the prognosis for patients.

References

1. Erbel R, Alfonso F, Boileau C, et al. Diagnosis and management of aortic dissection. Eur Heart J, 2001; **22**(18):1642-81.

2. Khan IA, Nair CK. Clinical, diagnostic, and management perspectives of aortic dissection. Chest, 2002; **122**(1):311-328.

3. Criado FJ. Chimney grafts and bare stents: Aortic branch preservation revisited. Journal of Endovascular Therapy, 2007; **14**(6):823-824.

4. DeRubertis B, Lee JT. Comparison of fenestrated endografts and the snorkel/chimney technique DISCUSSION. Journal of Vascular Surgery, 2014; **60**(4):856-857.

5. Lee JT, Greenberg JI, Dalman RL. Early experience with the snorkel technique for juxtarenal aneurysms. Journal of Vascular Surgery, 2012; **55**(4):935-946.

6. Lobato AC, Camacho-Lobato L. Endovascular Treatment of Complex Aortic Aneurysms Using the Sandwich Technique. Journal of Endovascular Therapy, 2012; **19**(6):691-706.

7. Kasirajan K. Branched Grafts for Thoracoabdominal Aneurysms: Off-Label Use of FDA-Approved Devices. Journal of Endovascular Therapy, 2011; **18**(4):471-476.

8. Minion D. Molded Parallel Endografts for Branch Vessel Preservation during Endovascular Aneurysm Repair in Challenging Anatomy. Int J Angiol, 2012; **21**(2):81-4.

9. Shuja F, Kwolek CJ. Treating the paravisceral aorta with parallel endografts (chimneys and snorkels). Semin Vasc Surg, 2012; **25**(4):200-2.

10. Lepidi S, Piazza M, Scrivere P, et al. Parallel endografts in the treatment of distal aortic and common iliac aneurysms. Eur J Vasc Endovasc Surg, 2014; **48**(1):29-37.

11. Donselaar EJ, van der Vijver-Coppen RJ, van den Ham LH, et al. EndoAnchors to Resolve Persistent Type Ia Endoleak Secondary to Proximal Cuff With Parallel Graft Placement. Journal of Endovascular Therapy, 2015; **23**(1):225-228.

12. Overeem SP, Boersen JT, Schuurmann RCL, et al. Classification of gutter type in parallel stenting during endovascular aortic aneurysm repair. Journal of Vascular Surgery, 2017; **66**(2):594-599.

13. Franklin RN, Silveira PG, Timi JRR, et al. Tomographic Measurement of Gutters and Analysis of the Conformability of Stent Grafts in the Octopus Technique for Endovascular Thoracoabdominal Aneurysm Repair. Annals of Vascular Surgery, 2016; **33**:202-209.

14. Mestres G, Uribe JP, Garcia-Madrid C, et al. The best conditions for parallel stenting during EVAR: an in vitro study. Eur J Vasc Endovasc Surg, 2012; **44**(5):468-73.

15. Mestres G, Yugueros X, Apodaka A, et al. The best in vitro conditions for two and three parallel stenting during endovascular aneurysm repair. Journal of Vascular Surgery, 2017; **66**(4):1227-1235.

16. Tse KM, Chiu P, Lee HP, et al. Investigation of hemodynamics in the development of dissecting aneurysm within patient-specific dissecting aneurismal aortas using computational fluid dynamics (CFD) simulations. J Biomech, 2011; **44**(5):827-36.

17. Zhao XM, Li R, Chen Y, et al. Hemodynamic analysis of intracranial aneurysms using phase-contrast magnetic resonance imaging and computational fluid dynamics. Acta Mechanica Sinica, 2017; **33**(2):472-483.

18. Morbiducci U, Ponzini R, Gallo D, et al. Inflow boundary conditions for image-based computational hemodynamics: impact of idealized versus measured velocity profiles in the human aorta. J Biomech, 2013; **46**(1):102-9.

19. Raptis A, Xenos M, Georgakarakos E, et al. Comparison of physiological and post-endovascular

aneurysm repair infrarenal blood flow. Comput Methods Biomech Biomed Engin, 2017; **20**(3):242-249.

20. Tasso P, Raptis A, Matsagkas M, et al. Abdominal Aortic Aneurysm Endovascular Repair: Profiling Postimplantation Morphometry and Hemodynamics With Image-Based Computational Fluid Dynamics. Journal of Biomechanical Engineering-Transactions of the Asme, 2018; **140**(11).

21. Chen D, Muller-Eschner M, Kotelis D, et al. A longitudinal study of Type-B aortic dissection and endovascular repair scenarios: computational analyses. Med Eng Phys, 2013; **35**(9):1321-30.

22. Cheng Z, Juli C, Wood NB, et al. Predicting flow in aortic dissection: comparison of computational model with PC-MRI velocity measurements. Med Eng Phys, 2014; **36**(9):1176-84.

23. Cheng Z, Wood NB, Gibbs RG, et al. Geometric and flow features of type B aortic dissection: initial findings and comparison of medically treated and stented cases. Ann Biomed Eng, 2015; **43**(1):177-89.

24. Chen DD, Muller-Eschner M, von Tengg-Kobligk H, et al. A patient-specific study of type-B aortic dissection: evaluation of true-false lumen blood exchange. Biomedical Engineering Online, 2013; **12**.

25. Xiong J, Ge YY, Liu XP, et al. Use of the Octopus Endograft Technique to Reconstruct Renovisceral Arteries Arising From the False Lumen of a Rapidly Expanding Type B Aortic Dissection After Endovascular Repair. Journal of Endovascular Therapy, 2017; **24**(1):107-111.

26. Perktold K, ., Resch M, ., Florian H, . Pulsatile non-Newtonian flow characteristics in a three-dimensional human carotid bifurcation model. Journal of Biomechanical Engineering, 1991; **113**(4):464.

27. Pedley T, *The fluid mechanics of large blood vessels*. 1982.

28. Fung YC. Biomechanics. Circulation, 1996; **192**(10):1251.

29. Madhavan S, Kemmerling EMC. The effect of inlet and outlet boundary conditions in image-based CFD modeling of aortic flow. BioMedical Engineering OnLine, 2018; **17**(1):66.

30. Zhuo C, Wood NB, Gibbs RGJ, et al. Geometric and flow features of type B aortic dissection: initial findings and comparison of medically treated and stented cases. Annals of Biomedical Engineering, 2015; **43**(1):177.

31. Ab Naim WNW, Ganesan PB, Sun ZH, et al. Prediction of thrombus formation using vortical structures presentation in Stanford type B aortic dissection: A preliminary study using CFD approach. Applied Mathematical Modelling, 2016; **40**(4):3115-3127.

32. Xu H, Piccinelli M, Leshnower BG, et al. Coupled Morphological-Hemodynamic Computational Analysis of Type B Aortic Dissection: A Longitudinal Study. Annals of Biomedical Engineering, 2018:1-13.

33. De Bruin JL, Brownrigg JR, Patterson BO, et al. The Endovascular Sealing Device in Combination with Parallel Grafts for Treatment of Juxta/Suprarenal Abdominal Aortic Aneurysms: Short-term Results of a Novel Alternative. Eur J Vasc Endovasc Surg, 2016; **52**(4):458-465.

34. Mestres G, Yugueros X, Apodaka A, et al. The best in vitro conditions for two and three parallel stenting during endovascular aneurysm repair. J Vasc Surg, 2017; **66**(4):1227-1235.

35. Franklin RN, Silveira PG, Timi JR, et al. Tomographic Measurement of Gutters and Analysis of the Conformability of Stent Grafts in the Octopus Technique for Endovascular Thoracoabdominal Aneurysm Repair. Ann Vasc Surg, 2016; **33**:202-9.

36. Li ZL, Yin HH, Wang M, et al. Octopus Endograft Technique to Treat a Ruptured Thoracoabdominal Aortic Aneurysm. Journal of Endovascular Therapy, 2018; **25**(2):237-241.

37. Spear R, Hertault A, Van Calster K, et al. Endovascular Repair of Postdissection Aneurysms Involving the Thoracoabdominal Aorta and Arch. Journal of Vascular Surgery, 2017; **65**(6):202s-202s.

Table 1. Flow division in aortic branches

Case	Flow division [%] (flow amount in branches/inflow at ascending aorta)						
	FL	TL	CA	SMA	LRA	RRA	CIA
Normal aorta	-	-	7.65	8.75	4.36	2.46	51.1
Pre-octopus (11M)	64.1	14.5	7.78	8.26	3.13	3.53	55.8
Pre-octopus (1M)	40.3	37.8	17.3	17.51	9.09	7.26	27.1
Post-octopus (1W)	41.7	36.6	4.7	33.4	3.82	10.8	25.8
Post-octopus (6M)	39.9	38.7	2.32	34.3	3.79	9.71	28.9
Post-octopus (12M)	26.6	52.2	-	26.9	-	17.7	34.0

FL – false lumen, TL – true lumen, CA – celiac artery, SMA - superior mesenteric artery, LRA – left renal artery, RRA – right renal artery, CIA – left and right common iliac arteries

Table 2. Flow division in aortic branches for the optimized models

Case	Flow division [%] (flow amount in branches/inflow at ascending aorta)						
	FL	TL	CA	SMA	LRA	RRA	CIA
Normal aorta	-	-	7.65	8.75	4.36	2.46	51.1
Post-octopus (1 week)	41.7	36.6	4.7	33.4	3.82	10.8	25.8
L-2cm	43.7	34.0	8.58	31.8	3.67	9.71	24.5
L-3cm	48.9	29.3	19.1	27.5	2.68	7.91	21.7
L-4cm	48.9	29.1	18.8	27.2	3.14	8.67	20.7
L-5cm	49.7	27.8	20.8	26.1	2.92	7.54	20.8
L-6cm	50.0	28.0	21.1	25.8	2.88	8.38	19.9
L-7cm	50.8	26.7	21.3	26.3	3.22	7.15	20.1
L-8cm	50.8	27.2	21.2	26.4	3.07	8.11	19.3
L-10cm	51.4	26.7	21.6	26.1	3.40	7.59	19.3
D-1mm	41.9	36.2	16.4	22.0	3.31	9.82	26.7
D-2mm	33.5	44.8	11.0	17.6	4.61	12.0	33.0

FL – false lumen, TL – true lumen, CA – celiac artery, SMA - superior mesenteric artery, LRA – left renal artery, RRA – right renal artery, CIA – left and right common iliac arteries

L-xcm – extension of the SG head by xcm

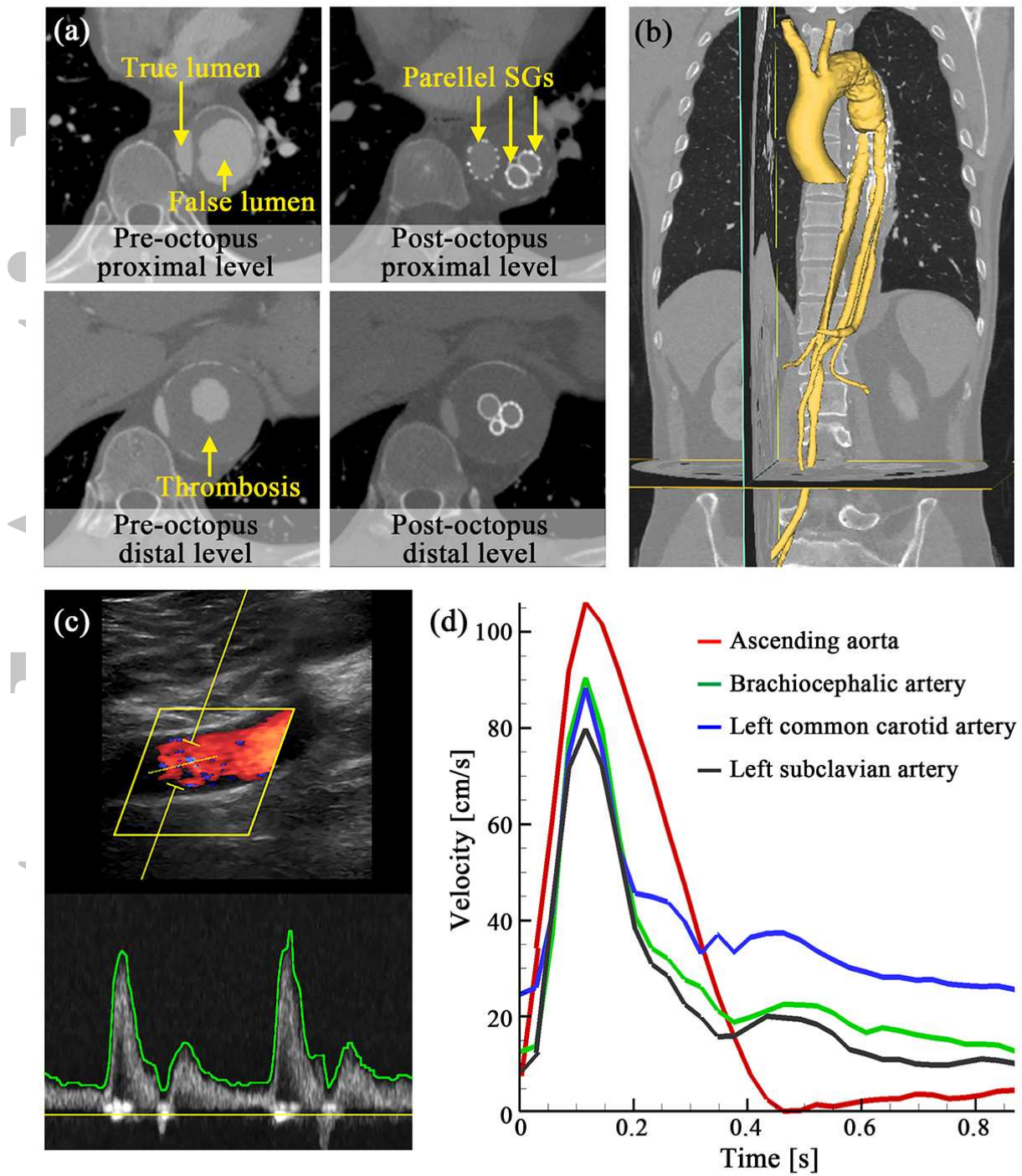D-xmm – reduction of the diameters of the limb SGs by xmm

Fig.1 (a) shows the representative slices of CTA datasets; (b) displays the 3-D reconstructed aortic model; (c) shows the Doppler ultrasound velocimetry; and (d) is the extracted velocity data as the velocity boundary conditions for the computational models.
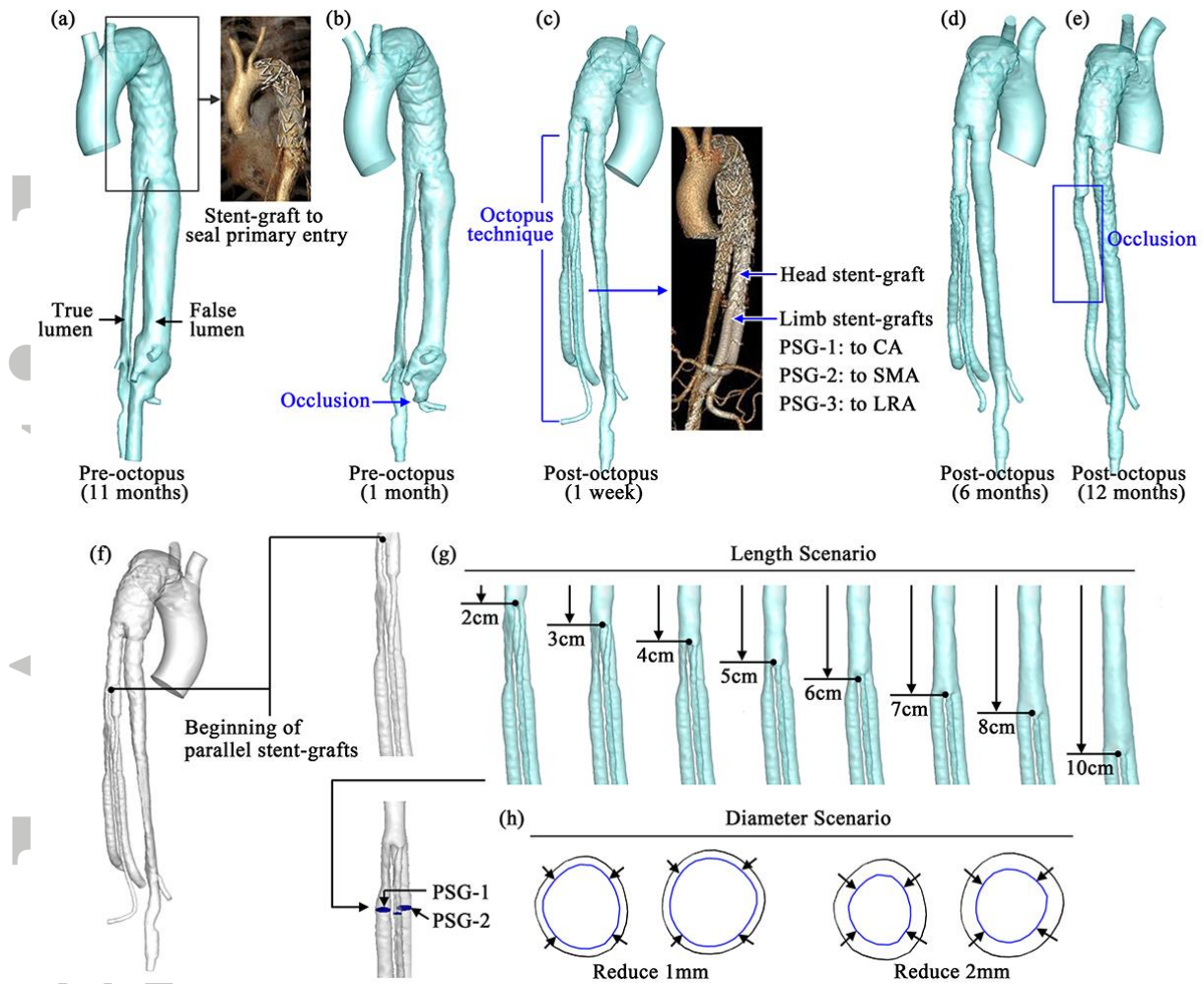
Fig.2 (a-e) shows the reconstructed models of the patient pre- and post-octopus treatment; (f) displays base model of SGs modification; (g) and (h) show the length and diameter scenario respectively.
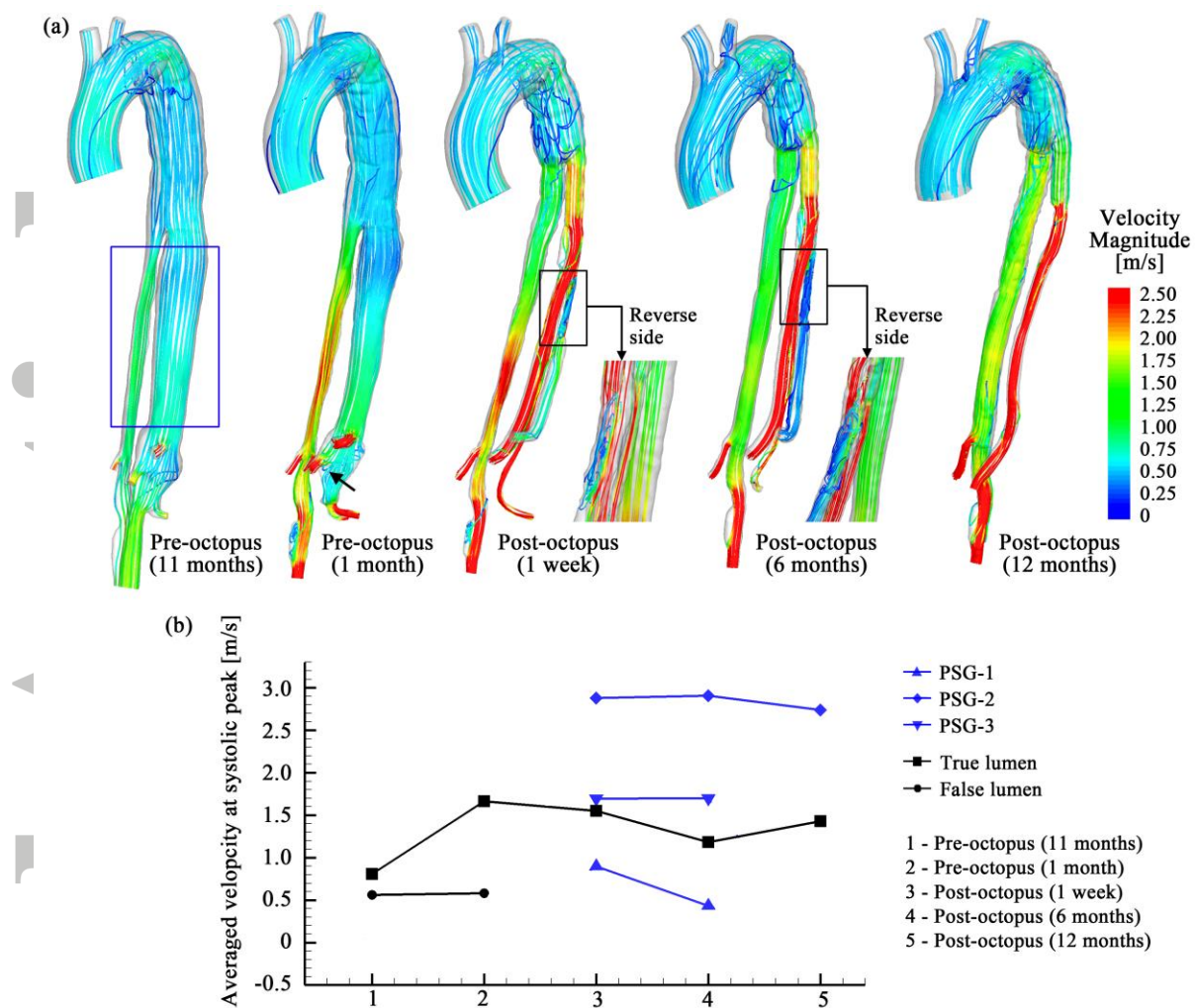
Fig.3 (a) shows the velocity streamline distributions at systolic peak in each pre- and post-octopus models; (b) shows the averaged velocity at systolic peak in each branches in the region of the blue square;
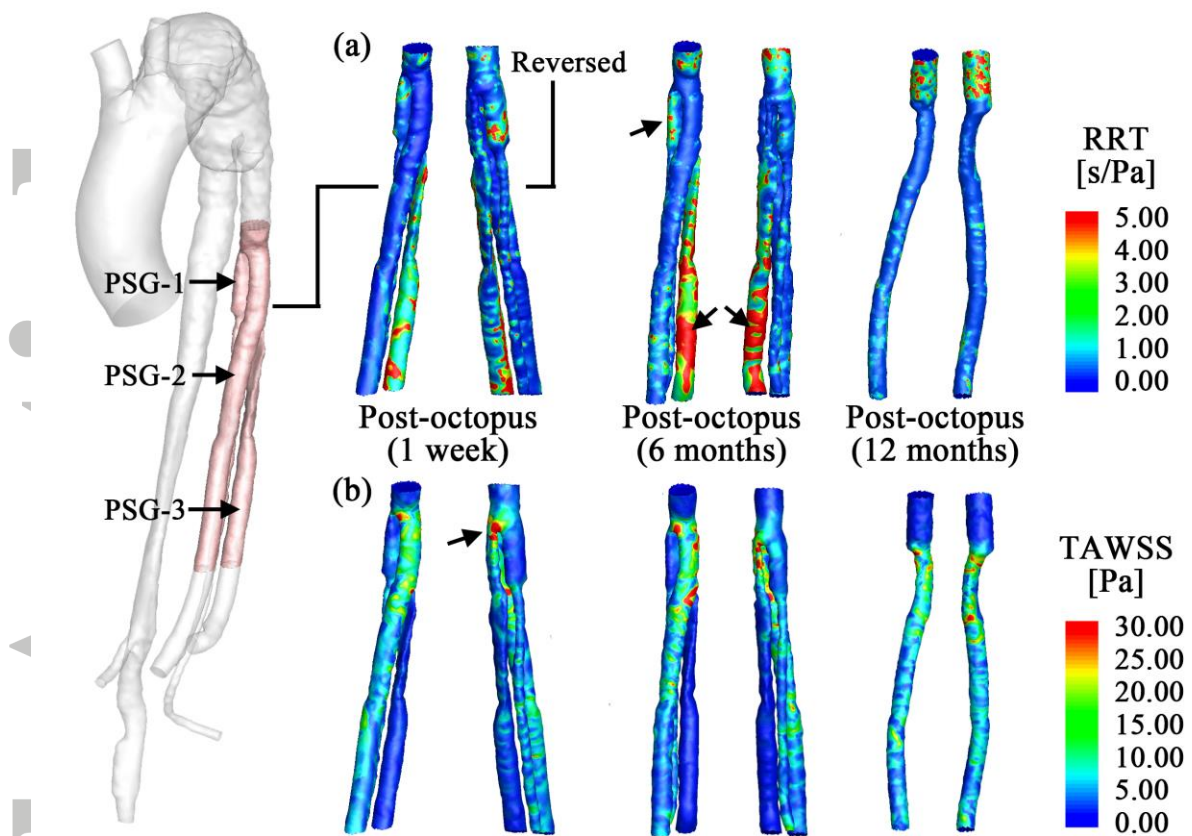
Fig.4 (a) and (b) respectively show the RRT and TAWSS distributions in the limb SGs post-octopus.
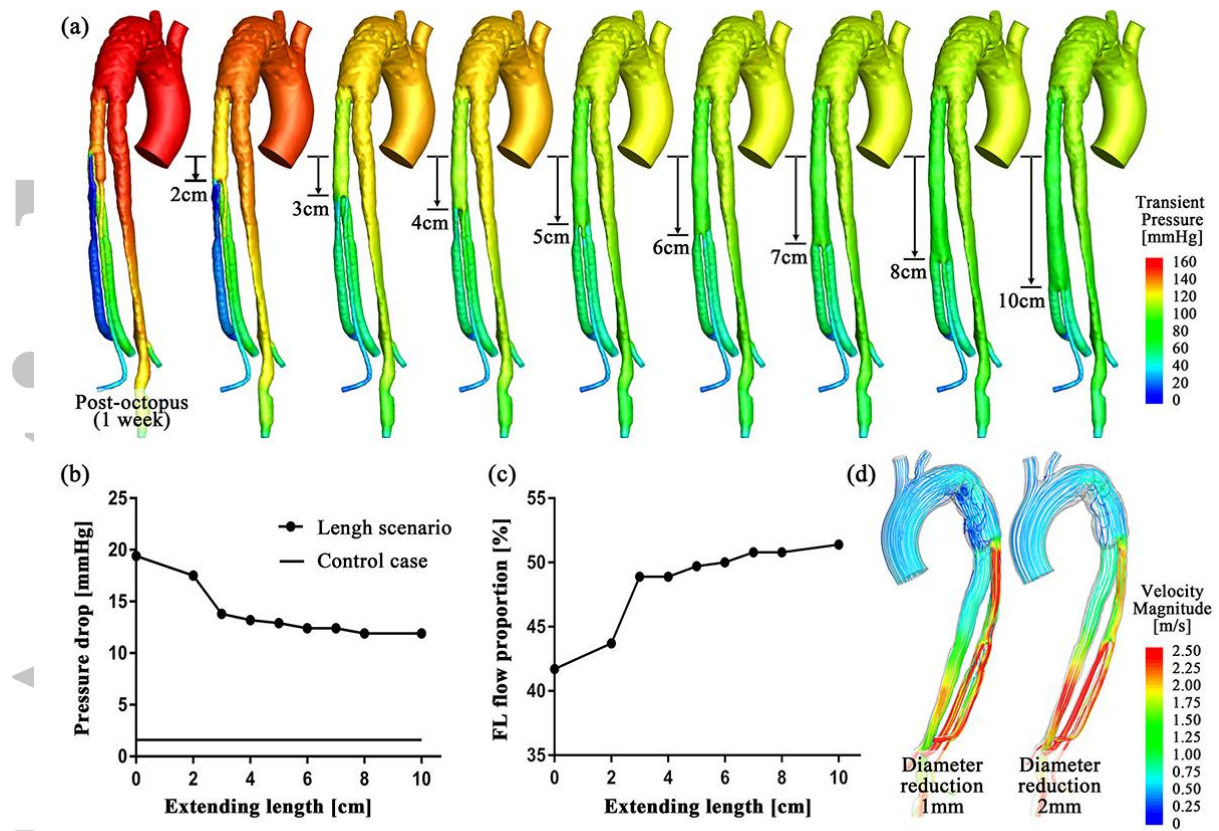
Fig.5 (a) displays the pressure distributions of the models of Length-scenario; (b) shows the pressure drop over an cardiac cycle of the models of Length-scenario as well as the control model; (c) shows the proportion of flow entering the original FL; (d) shows the velocity streamlines at systolic peak in the models of Diameter-scenario.

Mini-Abstract

The results indicate that when reconstructing the flow pathways via octopus stenting, it is important to ensure the flow distribution as physiological required with this new morphology. Position (or length) of the head-SG and diameter of the limb-SGs play an important role in controlling flow division, and high TAWSS around the head-SG acts as a main factor for graft immigration. This study, by proposing optimization suggestions with hemodynamic analyses for a specific case, implicates that pre-treatment SG scenarios may assist in wise selection and placement of the device and thus may improve long-term effectiveness of this kind of challenging endovascular repair techniques.

Graphical table of contents
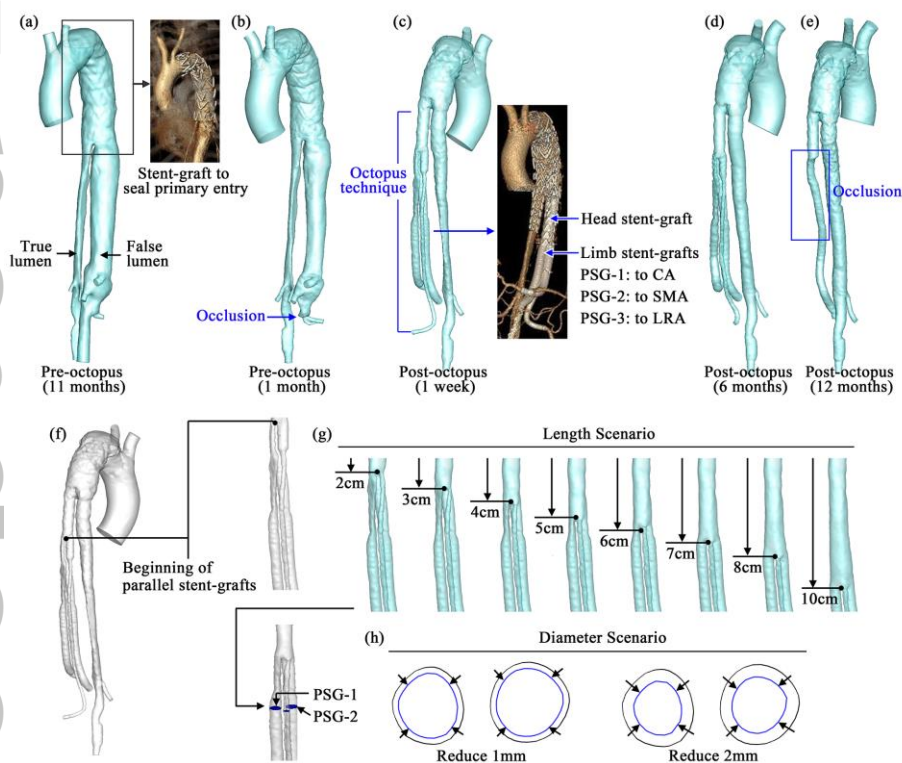
In this study, we established computational models based on CTA datasets of a patient who was treated by octopus stenting technique, with multiple post-treatment follow-ups(a-e). Hemodynamic condition was analyzed based on both the base models as well as optimized models. Suggestions for better stent-graft arrangement for this kind of complicated stenting technique, in order to better direct the blood flow, were proposed(g-h).